Received: October 14, 2025. Revised: November 12, 2025.

INASS

International Journal of
Intelligent Engineering & Systems

http://www.inass.org/

Low-complexity Deep Learning for Joint Channel-type Identification and SNR Estimation in MIMO-OFDM Using CNN–BRNN with LUT Labels

Yasmine M. Tabra[1]* **Furat Nidhal Tawfeeq[2]**

[1]*Department of Information and Communication, College of Information Engineering, Al -Nahrain University, Iraq*
[2]*University of Baghdad, Iraq*
* Corresponding author's Email: yasminetabra@nahrainuniv.edu.iq

Abstract: Channel estimation (CE) is essential for wireless links but becomes progressively onerous as Fifth Generation (5G) Multi-Input Multi-Output (MIMO) systems and extensive fading expand the search space and increase latency. This study redefines CE support as the process of learning to deduce channel type and signal-to-noise ratio (SNR) directly from per-tone Orthogonal Frequency-Division Multiplexing (OFDM) observations, with blind channel state information (CSI). We trained a dual deep model that combined Convolutional Neural Networks (CNNs) with Bidirectional Recurrent Neural Networks (BRNNs). We used a lookup table (LUT) label for channel type (class indices instead of per-tap values) and ordinal supervision for SNR (0–20 dB, 5-dB steps). The method was tested on Single-Input Single-Output (SISO), the 2×2 Alamouti space-time code, and 4×4 Quasi-Orthogonal Space-Time Block Coding (QO-STBC) in six standard situations: Nakagami fading, Log-Normal shadowing, Multipath fading, Gaussian, Rayleigh fading, and Rician fading. Channel identification was nearly perfect, and the SNR was robust, with most SNR errors being in adjacent bins indicating stable behaviour. The model reached 99.68% validation accuracy with 8.14×10^{-5} bit error rate (BER) and reduced complexity of 1.78×10^{8} for high order of subcarriers The method's novelty lies in accurate, low-complexity CE support from raw symbols and its demonstrated impact on end-to-end BER pilotless CE and SNR estimation to select equalizer without CSI reconstruction.

Keywords: Deep learning, MIMO-OFDM, Channel estimation, SNR estimation, CNN–BRNN, Alamouti, Space time block code, Quasi-orthogonal STBC (QO-STBC).

1. Introduction

Multi-Input Multi-Output (MIMO) communication uses more than one antenna at both the transmitter and receiver to make the connection more reliable and use the spectrum more efficiently without using more bandwidth or power [1, 2].

At the same time, Orthogonal Frequency-Division Multiplexing (OFDM) splits a high-rate stream into many narrowband subcarriers. This gives long symbol durations (which makes it more resistant to multipath), frequency-selective isolation of deep fades to a subset of tones, and flexible resource allocation for multiple users [2-6]. Because of these features, MIMO-OFDM has become a basic physical-layer technology and the waveform of choice for 5G systems that work over frequency-selective channels [7-9]. For coherent MIMO-OFDM reception to work, accurate channel estimation (CE) is very important because it makes equalization, detection, and decoding possible [10–12]. Traditional estimators like Least Squares (LS) and Mean-Squared Error (MSE) necessitate reliable channel state information (CSI) priors. Typically, calibrated regularization, interpolation, and pilot tones are employed [13, 14]. Conversely, an increase in the number of antennas can exacerbate these challenges due to time/frequency selectivity, multipath dispersion, inter-symbol interference (ISI), and variations in the signal-to-noise ratio (SNR).

Recent progress in deep learning (DL) has created new ways to directly infer CE and impairment from received complex samples. These new ways use architectures like Convolutional

Neural Networks (CNNs), Recurrent Neural Networks (RNNs), and Long Short-Term Memory (LSTM) models [15–18].

These networks have different numbers of layers, types of layers, activation functions, and ways of connecting them. They trade off inductive biases (like local convolutional structure or temporal memory) for model capacity and compute cost [19]. In a standard CNN stack, early convolutional layers extract localized spectral features, pooling layers offer limited invariance and down-sampling, and fully connected layers consolidate features for classification or regression; end-to-end training is executed via backpropagation to minimize a task-specific loss [20–22].

Motivated by these trends, this work investigates a learning-based front end for MIMO-OFDM that infers channel type and SNR directly from per-tone observations, without relying on CSI while preserving downstream BER performance.

RNNs demonstrate superior performance in processing sequential data, particularly in the context of time-series analysis. It can identify patterns and temporal relationships in sequential data by retaining a memory of previous inputs through hidden states [23]. RNNs and CNNs update hidden neuron weights based solely on past inputs, whereas BRNNs function in both forward and backward directions. Consequently, weights are adjusted according to historical and prospective learning outcomes [19, 24].

The prediction was generated by employing a variety of SNR values, ranging from 0 dB to 20 dB. The performance of the DL-aided CE is compared to other approaches in the literature using MMSE and BER against SNR criteria. The proposed DL front end gets channel class and SNR directly from Y(k) without having to rebuild CSI. It then uses these estimates to set up the normal receiver chain (like MMSE equalization and carrier-phase estimation (CPE)), which may use standard pilot-based H like in baseline systems.

This paper is structured as follows: Section 2 presents the related research in the domain of CE-based DL. In Section 3, the dataset generation and description and in Section 4, 5G MIMO-OFDM model. While pilotless DL based estimation design is suggested to help with these problems located in section 5. Section 6 presents simulation results that evaluate the effectiveness of the proposed techniques and compare them with existing literature-based research. Finally, section 7 outlines the main conclusions of the paper.

2. Related Works

Meena Lakshmi, et.al in 2022 [17], compared CE using different DL approach in 5G MIMO-OFDM systems. They showed that there is an increasing opportunity to enhance CE by using DL algorithms to reduce the complexity of traditional CE methods as moving towards massive MIMO increase the number of antennas and hence the transmitted data size making as extra cost of the pilot symbols used for CE go up.

In 2022 [25], A.K. Nair and V. Menon used pilot based CE with compression sensing and BLSTM networks to improve the performance of symbol detection and minimize BER. The proposed model compared to traditional LMS and MSE using a limited number of pilot symbols and showed advance in performance.

In 2023 [15], D. Adolfsson conducted an investigation into the application of CNNs based CE in 4x4 MIMO-OFDM with QPSK symbol modulator. The result was compared with traditional methodologies and showed that the CNN achieved BER similar to LMS but higher than MMSE by 80% with zero symbol error rate (SER) tested under EYE flat fading channel at SNR equal to 20 dB.

The DL method was developed by M. Wang, et.al, in 2023 [26] estimated the OFDM channel by making use of a low-resolution image that was formed from the LS channel matrix and CSI, which is considered to be a high-resolution image combination. For simulation 16 pilots were used modulated with QPSK and tested under Nakagami with AWGN channel.

Z. Sh. Hammed and S. Y. Ameen in 2023 [27], employed a DL network for LSTM in the CE approach. They compared the results of this technique to those of more standard methods such as MMSE and LS with 8 and 64 pilots and showed that lower number of pilots achieved better CE accuracy than traditional methods.

In 2024, M. Qasaymeh et al. [28] used several CNNs to estimate CSI in the MU-MIMO channel. The CNN went through a long training and testing process with grayscale images as inputs for the model. The training dataset contains from 2 to 10 pilot blocks used in the estimation. This technique achieved a normalized root-mean-square error similar to LS with lower SNR level.

In their 2024 study, Y. Singh et al. [29] analysed the DL-based computational efficiency model, which utilizes image processing techniques to achieve a high degree of precision in computational efficiency. The researchers generated 5G data to enable the training of a CNN model, hence

facilitating its ability to learn and identify patterns related to Single Input Single Output (SISO) channels and managed to improve accuracy and robustness with reduce dependence on pilot estimates.

In 2024, S. Deepanjali et.al. [30] employed student-teacher architecture to train CNN for CE-based pilot signal. The model was tested against known attacks and manged to reduce attacks success rate to 0.06 with MSE 0.029 after 100 epochs.

S. Vasa, et.al in 2024 [31], looked at the level of mobility shown by Doppler effects in MIMO system with a multi-path channel in 5G and future networks. Authors suggested a hybrid LSTM-CNN architecture that showed reduction in MSE and BER compared to LS with different pilot number and varying in doppler effect.

G. Villemaud and M. Mallik in 2025 [32], used convolutional neural tangent kernel (CNTK) to relate missing channel matrix and estimate the channel response from known pilots location. This method reduced memory usage by reducing the size of dataset required for CE using previous works. The simulation achieved high accuracy estimation with 1.48 × 10−4s and using only 1.2 GB of random-access memory (RAM).

A. Rakhmania, et al. in 2025 [33] compared different CE algorithms by mean of their advantages and disadvantages. The comparison was made between several machine learning-based CE algorithms and showed their advances in reducing pilot overhead, increase accuracy, and adaptability to change in channel conditions. The comparison included complexity comparison with traditional CE algorithm.

An examination of the literature shows that several authors have used different DL models for CE in MIMO-OFDM systems. These models achieved similar accuracy to conventional CE algorithms (i.e., LS and MMSE) with a smaller number of pilots used. They managed to reduce the complexity of CE but still relying on pilots to perform the estimation which reduces the spectral efficiency and overall throughput. Another aspect that wasn't considered in all previous works is the effect of noise level affecting the transmitted signal and its role in biasing the decision in CE.

This work employs the first DL model from six channel characteristics (Nakagami Fading, Log-Normal Shadowing, 3-tap Multipath Fading, Gaussian, Rayleigh Fading, and Rician Fading) that have not been thoroughly investigated in existing literature to predict channel types. The reduction in aspect. This employs a lookup table (LUT) that contains channel responses, utilizing their respective indices as training targets. The second DL model predicted the SNR level that affected the transmitted signal.

Table 1. Related works comparison

Method	Pilots-based	Noise effect
LS	Yes	Highly sensitive to noise with no SNR used
MMSE/ LMMSE	Yes	Highly effect decision and SNR aware
CS-based	Yes	Fails at low SNR
DL-CSI	Yes	Embedded SNR
This work	No	Predict SNR

Eliminating noise from the received signal before processing on the receiver side will improve the overall accuracy of the system and decrease the BER. DL based CE depends on noise power prediction, which greatly improves model performance, adaptation, and resilience. In wireless communication systems, additive noise, channel effects, and the received signal together define the transmitted signal. A DL model may misinterpret noise as the real signal in cases when the noise power is either unknown or incorrectly estimated during training or inference, so producing unsatisfactory CE. Accurate noise power estimate helps the model to distinguish between signal and noise, so improving knowledge of channel properties. Also helps the network to modify its estimate and feature extraction techniques in line with the current SNR and improves the training process by means of loss function weighting or normalizing. Table 1 summarize related work and shows that related works estimates the H unlike our approach that estimates the channel type and uses corresponding channel response from LUT. Also estimate SNR to help receiver choose proper equalizer for stable accuracy across all noise levels.

3. Dataset Generation

We created jointly a supervised dataset to train a dual-head deep network that can tell the channel type (Rayleigh, Rician, Nakagami, Log-Normal, Gaussian, Multipath) and the SNR index of the Eb/N0 grid from 0 to 20 dB in 5 dB step (6 classes) just from frequency-domain received samples. We store SNR index in {0...4} rather than a float.

We support three types of transmitters: SISO (1x1), Alamouti 2x2 (orthogonal STBC), and QO–STBC 4x4. Random bits are mapped QPSK (4–QAM) symbols. For Alamouti and QO-STBC, symbols are mapped into codewords with the usual

orthogonal/QO structure, and codewords are normalizes power across transmitting MIMO antennas. Propagation is generated from six canonical fading models. Flat channels are held constant across subcarriers and then tiled over k, while the multipath case is transformed to frequency domain H by FFT. AWGN is added with targeted SNR value.

That dataset labelling for channel types is as follows: {0: Rayleigh, 1: Rician, 2: Nakagami, 3: Log-Normal, 4: Gaussian, 5: Multipath}, SNR labelling are {0: 0 dB, 1: 5 dB, 2: 10 dB, 3: 15 dB, 4: 20 dB}; while MIMO mode are {0: SISO, 1: Alamouti2, 2: QO–STBC4}. Table 2 include the LUT for different channel types. The final database comprises 230,814 samples, organized into 38,469 per channel and 32,778 per SNR for the SISO configuration. In the case of the Alamouti 2x2, the dataset contains 127776 sample with 21296/19140 per channel/SNR, respectively.

For the QO-STBC configuration, there are 41,862 samples, distributed as 6,977 and 7,314 per channel and SNR. The samples are categorized into Real/Imaginary stacking and accompanied by a one-hot label to facilitate the training of a CNN-BRNN model, which aims to predict both the channel and SNR class simultaneously. The feature length per sample in the SISO/Alamouti 2x2/QO-STBC 4x4 dataset varies, comprising 64, 256, and 1024 features, respectively.

A new testing dataset was created using a distinct random seed to avoid overlap with the training dataset. Each record in the test set retains an identifier for (channel type, SNR level, noise seed), and in instances of duplicate identifiers, the record is removed from the set and a new one is generated. The size of the test set fluctuates based on the MIMO setup mode. The SISO test set has 1,703 samples; the Alamouti 2x2 set consists of 1,148 samples; and the QO-STBC 4x4 set includes 581 samples.

Table 2. Lookup Table (LUT) for different Channel types

Index	Channel Type
0	Rayleigh Fading
1	Rician Fading
2	Nakagami Fading
3	Log-Normal Shadowing
4	Gaussian
5	Multipath Fading

4. System Model

This work examines a N_T x N_R MIMO-OFDM channel model over 5G, that is N_T and N_R represents the number of antennas in transmitter and receiver respectively. The model depicted in Fig. 1 shows the transmitter, channel, and receiver.

4.1 Transmitter Side

Generate stream of bits and put them into time slots groups of k. k = 1, …, $log_2 M$, where M is the modulation order. The data vector x(k) with M modulated symbols is represented by:

$$x(k) = [x_1(k), x_2(k), \dots, x_M(k)] \quad (1)$$

Different modes of modulation were investigated in this paper; the Quadrature Phase Shift Keying (QPSK) with M=4, and quadrature amplitude modulation (QAM) with M=16 or M=64.

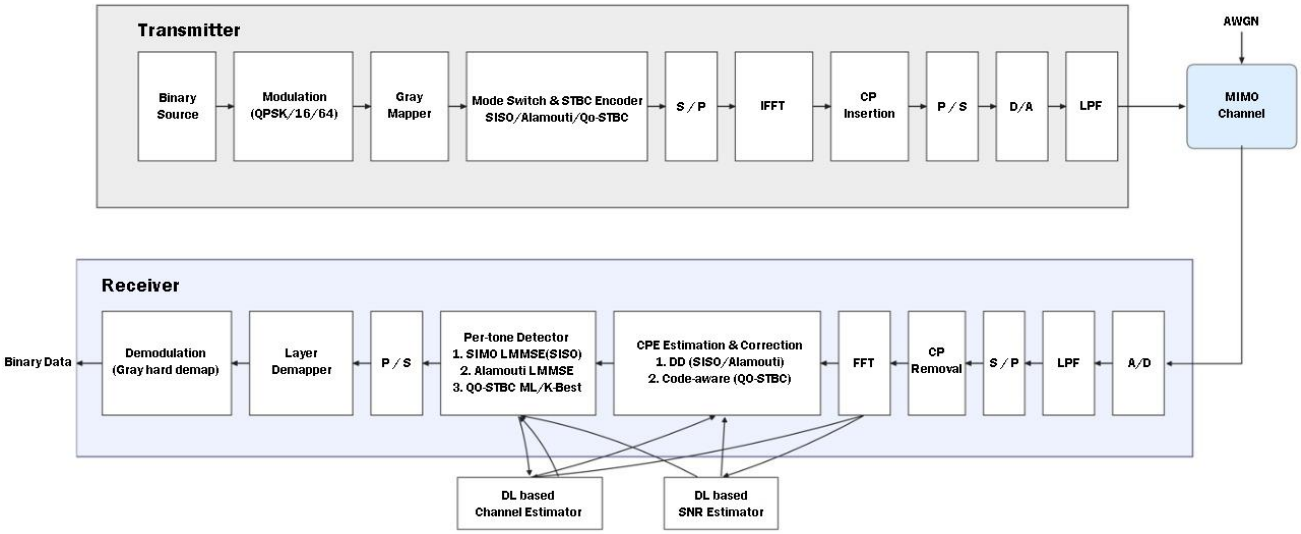

Figure. 1 MIMO-OFDM system with DL models

Then, use Gray-coding to map them. This method makes sure that adjacent symbols differ by only one bit, which lowers the hard decision BER. The IFFT is then applied to each antenna, which packs symbols onto N_{FFT} subcarriers (i.e., N_{FFT} represent the number of tones per OFDM symbol (per time slot)).

$$\hat{x}_p(n) = IFFT\{x_p(k)\} \quad (2)$$

To avoid ISI, a CP is added at the end of each symbol. This is usually done by appending the last. N_c samples to the beginning of the symbol. Now the signal $\hat{x}_{cp}$ can be described as

$$\hat{x}_{cp}(n) = \begin{cases} \hat{x}_p(n+N), & else \\ \hat{x}_p(n), & n = 0, 1, \dots, N-1 \end{cases} \quad (3)$$

As for Space-time coding three mode where used based on the number of N_T x N_R. These modes are:

A. **SISO mode with (1x1) in this case** no coding is required just parallel streaming.
B. **Alamouti** orthogonal STBC with (2×2) [34] in this case it uses the coding matrix $\begin{bmatrix} x_1 & x_2 \\ -x_2^* & x_1^* \end{bmatrix}$, where (*) denotes the complex conjugate.
C. **QO-STBC(4×4)** [34, 35]**:** with 4-slot block mixing $[\, s_1 .. s_4]$ and conjugates. This will provide 4-branch diversity at high rate near 1

4.2 Channel mode

5G MIMO-OFDM channel model with different N_T x N_R proposed in this research. After coding steps, each codeword row is scaled by $1/\sqrt{(N_T)}$ so total transmitted power is mode-invariant to allow fair SNR comparisons. In this research, *H* represents the complex path gain of the channel and it is almost static across the code block for STBC (Alamouti 2×2, QO-STBC 4×4).

Six different types of channel responses have been exploited in this paper; these are:

1. Rayleigh Fading Channel: $H_{(r,t)}(k) \sim \mathbb{CN}(0,1)(rich\ NLOS)$ [36]
2. Rician Fading Channel: LOS + diffuse, K-factor controls LOS strength [37].
3. Nakagami-m: envelope shape m (from severe to mild fading) [38].
4. Log-Normal: large-scale shadowing with dB spread σ_{dB} [39].
5. Gaussian (i.i.d. complex): $\mathbb{CN}(0,1)$ entries (robustness class) [40]**.**
6. Multipath (frequency selective): L-tap $\mathbb{CN}(0, p_\ell)$, FFT to H[k] [41].

4.3 Receiver side

The received signal at antenna Rx_i, and with time slot *t* per subcarrier *k* is represented by:

$$y_{r,t}(k) = \sum_{n=1}^{N_t} \hat{X}_{cp(t,n)}(k).H_{(r,n)}(k) + \omega_{(r,t)}(k) \quad (4)$$

$\omega_{(r,t)}(k)$ represents the AWGN to simulate the noise affecting the signal during transmission. The noise variance was calculated as $N_0 = \frac{1}{K.SNR}$, for rage of SNR staring from 0 to 20 dB.

The initial process at the receiver involves converting serial data into parallel format. Subsequently, the removal of the guard interval is employed to mitigate the ISI effect. CPE is modelled per time-slot t as a linear phase across subcarriers.

$$y_{r,t}(k) = e^{j(a_t + b_t k)} \sum_{n=1}^{N_t} \hat{X}_{cp(t,n)}(k) H_{(r,n)}(k) + \omega_{(r,t)}(k) \quad (5)$$

The (a_t, b_t) is estimated to denote the actual $y_{r,t}(k)$. different strategies are used based on STBC mode used:

A. **SISO/Alamouti:** decision-directed (DD) MMSE equalization

$$W = (H^H H + \lambda I)^{-1} H^H \quad (6)$$

and $\tilde{s}_t = W y_t$, then scaled by $\frac{1}{\sqrt{N_t}}$. hard decision of $\hat{s}_t$ from $\hat{\rho}_t(k) = \hat{s}_t^H \tilde{s}_t$ with phase $\phi_t = \angle \rho_t$ and weight $w_t = |\rho_t|$, and fit a **weighted least-squares** line $\phi_t(k) \approx a_t k +, b_t$ (using reliability gates vs. d_{min} and channel gain)

B. **QO-STBC:** we enhance code awareness by tentatively decoding $\hat{s}(k)$, then re-encode $\hat{X}(k)$. Predicting $\hat{y}_t = H\hat{X}_t$, and estimate phase from $\rho_t(k) = \hat{y}_t^H y_t$; incorporating a relative-error gate prior to the same LS fit. We conduct CPE exclusively when the measured slope is significant (for instance, in cases of multipath or SFO). We set λ to be approximately equal to N_0, and as a result, we effectively eliminate residual CFO/SFO phase, remove the mid-SNR "hump," and achieve

noticeable improvements in BER. This is particularly relevant for higher-order QAM.

The subsequent step is the Per-tone detection phase, which converts the CPE-corrected received samples into the transmitted symbols associated with each OFDM subcarrier k. OFDM converts the frequency-selective channel into a diagonal structure, signifying that the subcarriers demonstrate a level of independence from each other. This is the approach by which we can ascertain tone. The way it works differ according to modes mentioned earlier:

A. SISO: single symbol for each tone utilizing an MMSE combiner

$$\hat{s}_k = \frac{h_k^H y_k}{\left|\left|h_k\right|\right|^2 + \lambda}, \lambda \approx N_0 \quad (7)$$

with $N_R > 1$ this is noise-aware MRC

B. Alamouti 2×2: Orthogonality serves to decouple the two symbols, resulting in a closed-form combiner.

$$\hat{s}_{1,k} = \frac{\sum_r (h_{1,r}^* y_{0,r} + h_{2,r} y_{1,r}^*)}{\sum_r \left(\left|h_{1,r}\right|^2 + \left|h_{2,r}\right|^2\right) + \lambda}, \quad (8)$$

$$\hat{s}_{2,k} = \frac{\sum_r (h_{2,r}^* y_{0,r} + h_{1,r} y_{1,r}^*)}{\sum_r \left(\left|h_{1,r}\right|^2 + \left|h_{2,r}\right|^2\right) + \lambda} \quad (9)$$

C. QO-STBC 4x4: Symbols are interconnected, allowing for the simultaneous detection of the 4-vector. For QPSK, we can get accurate maximum likelihood by enumerating 4-tuples s and selecting the shortest Euclidean distance $\sum_t \left|\left|y_{k,t} - H_k x_t(s)\right|\right|^2$.

For 16/64-QAM, we construct the real system represented by $y = Gx + n$. Subsequently, perform the QR factorization on G and execute the sphere/K-Best search on the triangle R, which eliminates candidates while remaining close to maximum likelihood. Permutes variables to cluster the most dependable components, then employing K_{best} real PAM levels $A_{real}$to retrieve $\hat{s}_1, \ldots, \hat{s}_4$..

The detector uses N_0 as the MMSE regularizes λ (and to scale metrics). To compute LLRs, a common approximation per bit b is

$$LLR(b) \approx \frac{1}{N_0}\left(\min_{s:b=0} \mathcal{M}(s) - \min_{s:b=1} \mathcal{M}(s)\right) \quad (10)$$

with $\mathcal{M}$ the whitened Euclidean metric from the detector; even when making tough choices, the distances from the detector affect DD-CPE gating and DD channel-estimation reliability. After FFT and CPE, the pipeline placement runs for each subcarrier: equalize/combine using H_k and $N_0$to get $\hat{s}_1$, and then demap to bits (or LLRs). In the DD (pilotless) case, its outputs go back to update $\widehat{H}_k$ (and $\widehat{N}_0$) for the next iteration. This means that good per-tone detection makes the whole receiver better.

Finally, Nearest neighbour to the known constellation, then inverse Gray LUT to bits. *For* fast, vectorizable decisions.

5. Pilotless DL-based CE and SNR

Prior studies concentrated on estimating the channel response by utilizing the received signal as input and the channel response as output for the DL model. The presence of complex numbers in both the received signal and the channel response introduces additional complexity to the estimation method. This research will examine the application of LUT for channel response to address this issue. Each channel type will be assigned a unique index, and the DL model will estimate the index for each channel. The table below presents the indexing of the channel responses to be estimated in this study. Utilizing the LUT channel response, rather than estimating the complex response values, enhances decoding accuracy by employing a matched channel response consistent with that used in the encoder.

This approach also decreases the estimation complexity associated with complex response values, thereby minimizing training and estimation time. The transmitter and receiver will possess identical versions of the LUT.

Table 3 lists all the architecture setup of the proposed CNN-BRNN model. The produced dataset will constitute the basis for training the DL model. First, the training dataset was split so that 80% is used for training and 20% for validating using fixed random seed in all runs to ensure determinism. The received signal is expressed as a complex number (i.e., $A + iB$). The initial phase entails the separation of the transmitted signal into its real and imaginary components. The [A, B] pair is normalizer using per sample Root Mean Square (RMS) functions. All samples are appended before data splitting for training and validation subsets. As for the testing phase, a new test data will be generated for this task.

The proposed CNN-BRNN was trained for 100 iterations with an adaptive learning rate of 0.001 and weight decay mechanism by 1e-5 incorporating Reduce-on-Plateau schedular. The training and validation datasets are batches in 32 size to training

Table 3. Setup and training hyperparameters

Parameter	Specification
Seed	Random
Training dataset split	80%
Testing dataset split	20%
Optimizer	Adam
Optimizer Learning rate	3×10^{-3}
Optimizer weight decay	10^{-5}
Loss	Categorical Cross entropy
Batch size	32
Max epochs	100 (both tasks)
LR schedule	Reduce-on-Plateau
LR minimum rate	10^{-6}

Table 4. Layer types of proposed CNN-BRNN

Layer Type	No of Filters	Filter size	Dropout rate	AF
Input	-	-		he_normal
Conv1D + BN	32	5	35%	ReLU
Conv1D + BN	16	5	35%	ReLU
BRNN	16	-	35%	-
Max Pool		-		-
Dense	16	-	50%	ReLU
channel index	6	-		SoftMax
SNR index	5	-		SoftMax

the model for 100 epoch using Adam optimizer and Categorical Cross entropy loss function. The training model will utilize the received signal as input, producing two outputs: the first denotes the index of the channel response, and the second represents the SNR. The layers of the proposed DL model utilized for estimating various channel responses, along with their parameters, are presented in Table 4. The proposed model incorporates a combination of CNN and BRNN layers, each defined by unique parameters.

Every convolutional layer uses the ReLU activation function (AF), and then batch normalization (BN) follows. There is a max pooling procedure after the BRNN layer, producing 16 outputs. At last, a fully connected layers will create six distinct outputs, each matching a different index in the channel type replies to LUT.

Trained on labels connected to the SNR for the same input pairs, the same model produces an extra five outputs matching SNR index in LUT. Every one of these outputs denotes a particular SNR range. The channel response ultimately corresponds with the calculated index during the decoding of the received signal, after the removal of transmission-induced noise.

Table 5. Accuracy of CNN- BRNN model under different MIMO Configuration

Estimator Task	MIMO Size	Training	Validation
Channel	1x1	100%	100%
	2x2	98.38%	99.68%
	4x4	96.85%	99.72%
SNR	1x1	93.98%	97.24%
	2x2	81.67%	82.93%
	4x4	80.34%	82.04%

6. Configuration and simulation results

The system was modelled using a processor from the 12th generation of Intel, the Core i7-1255U, and 8 GB of RAM. Python version 3.11 is used to run the programming for the DL model, as well as the transmitter and the receiver. Table 5 displays the training and validation accuracy results for CE and SNR prediction for (1x1, 2x2, or 4x4) MIMO channels.

In Alamouti (2×2) and (4×4), the trend continues with slightly slower convergence as dimensionality and space time mixing increase, but validation still plateaus around 99–100% and training settled a few points lower (96–98%). The consistent Val > Train gap shows that the model is being intentionally conservative by using per-sample RMS normalization, label smoothing, and dropout. This means that the model is underfitting rather than overfitting, which is why it generalizes so well. As for SNR estimation, the accuracy goes up quickly and then levels off for SISO, Alamouti, and QO-STBC.

The highest accuracy is for SISO and the lowest is for STBC modes, which is due to the extra symbol mixing. Label smoothing and regularization, not overfitting, often make validation longer than training. Confusions are concentrated between adjacent SNR bins (e.g., 10↔15 dB), in line with ordinal targets. The decision-directed CPE step makes estimates more accurate on multipath, especially at mid/high SNR. The curves show that convergence is stable after about 60 to 100 epochs and that generalization is strong.

Confusion matrices (CM) for testing data are another performance metric. Fig. 2 displays the testing CM for the seven channel models and five SNR levels that comprise the proposed CNN-BRNN model. The accuracy curves and the CM together show where misclassification occur. The maps are almost diagonal across SISO, Alamouti, and QO-STBC for channel identification. The few entries that are not on the diagonal are mostly between

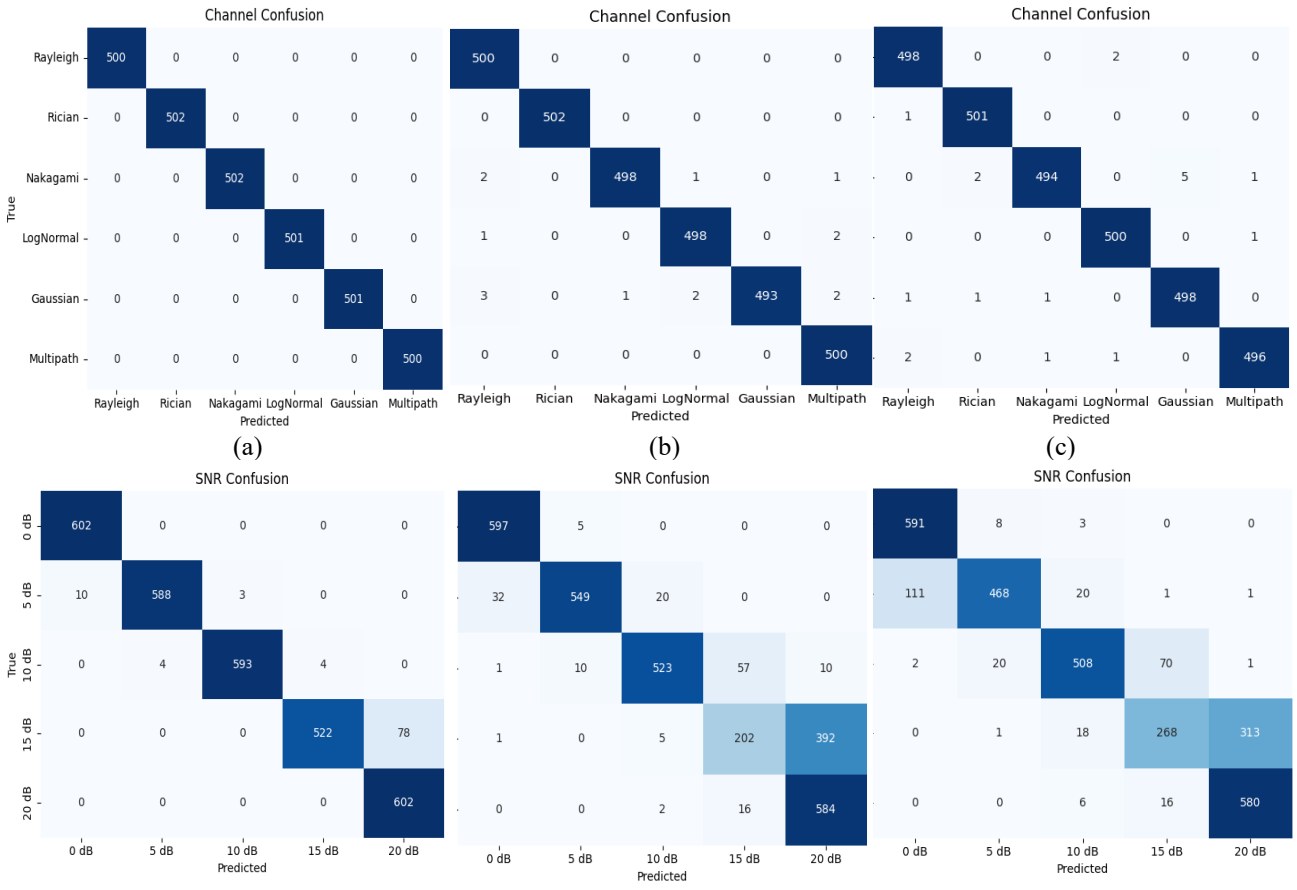

Figure. 2 Testing CM for proposed CNN-BRNN estimation: (a) SISO (1x1) channel, (b) Alamouti (2x2) channel, (c) QO-STBC (4x4) channel, (d) SISO (1x1) SNR, (e) Alamouti (2x2) SNR, and (f) QO-STBC (4x4) SNR

Nakagami, Log-Normal, and Gaussian. This means that the fading statistics in the learned feature space are overlapping, not that there is a lot of misclassifications. When estimating SNR, the errors are mostly upward (e.g., 15→20 dB) and not symmetric. This suggests that the decision surface has a slight high-SNR bias. These patterns show that the problem of channel separability has mostly been fixed by the current preprocessing.

The proposed CNN-BRNN model with CORAL (COnsistent RAnk Logits) method is used to test SNR per class CM after mapping bins to mid-point. The model achieved a validation accuracy of 92.3% with increment by 3% and reduced Mean Absolute Error (MAE) to 1.317 dB compared to 1.5 dB for original SoftMax based model at 2x2 MIMO.

The model maintains strong ordinal calibration with minimal cross-bin confusion. For SNR values with mid-point 2.5 dB and 7.5 dB demonstrate high identification recall. In contrast, higher SNR mid-points 17.5 and 22.5, introducing an overlap between adjacent classes due to feature similarity. This results that SNR estimation suitable for real-ime adaptive equalization by guiding direct selection of proper modulation, and coding scheme. The ±1 bin misclassification degraded the equalizer accuracy to less than 0.2 dB.

Table 6. per class CM and MAE for SNR estimation

MIMO Mode	Accuracy	MAE (dB)	Worst-Class Δ (dB)
1×1	91%	1.05	±0.8
2×2	92%	1.32	±1.0
4×4	90%	1.47	±1.3

Table 6 shows per class confusion and MAE for each MIMO mode, with validation accuracy using CORAL after 100 epochs.

The accuracy of the prediction at the receiver side for the three MIMO configurations is shown in Fig. 3. As expected, the accuracy of predictions increases as SNR increase. This is especially true for lower-order modulations like QPSK, which is much more accurate at low SNR than 16-QAM and 64-QAM. The accuracy performance also gets better with 4×4 than 2×2 and 1×1 structures because they have more spatial diversity and better symbol separation. Channels like (Gaussian and Rician) are

the most accurate because they either have less fading or a line-of-sight component.

On the other hand, (3-tap multipath and Rayleigh fading) are less accurate, especially for higher-order QAM when the SNR is low. In the 4×4 case, QPSK keeps getting better, but the accuracy level for higher-order modulations shows that the benefits are getting smaller because of how complicated the modulations are and how sensitive they are to noise. The MIMO-OFDM system simulation parameters considered in simulation this project is presented in Table 7.

Three distinct modulation modes were evaluated for each MIMO configuration and channel characteristic.

In Fig. 4 for each Eb/N0 point, we used 6,400, 12,800, and 19,200 transmitted bits for contrasts QPSK, 16-QAM, and 64-QAM, respectively, across various channel characteristics for MIMO configurations of 1x1, 2x2, and 4x4 and for all channel types. Except for Multipath channel where the used number of transmitted bits increased to 14,080, 28,160, 42,240 for QPSK, 16-QAM, and 64-QAM, respectively, to reduce the confidence interval of frequency selective fading. The simulation doesn't provide early stopping option, such that each point meets specified number of bits.

The illustration indicates that QPSK yields the lowest BER at low SNR for fading channels (Rician, Rayleigh) without the necessity for CSI.

Table 7. OFDM system simulation parameters

Number of subcarriers	64
FFT length	64
CP	25%
Modulation method	QPSK, 16-QAM, 64-QAM
Number of multipath	3
Noise model	AWGN
SNR	0 to 20 dB
Number of Tx, Rx	1 x 1, 2 x 2, 4 x 4

In scenarios involving channel impairments such as fading and interference, QPSK frequently demonstrates a lower BER compared to higher-order QAM for the same SNR. The observed channel effects align with theoretical predictions, indicating that Gaussian and Rician channels demonstrate superior performance compared to Rayleigh, Nakagami, and Multipath fading environments.

The shaded band in figures indicates 95% Wilson confidence interval computed from observing the error count at each SNR. Points that showed zero error is reported as one sided upper bound 95% Wilson. We compared the results of the proposed system with some of the related works listed in Table 1 under similar simulation parameters Table 8 shows the BER comparison with conventional and DL-based pilot CE algorithm. The results shows that the proposed system reduced the BER over DL methods using 9 pilots by 57.16% (2.33x lower BER). Table 9 includes a complexity comparision by mean of Floating Point Operation per second

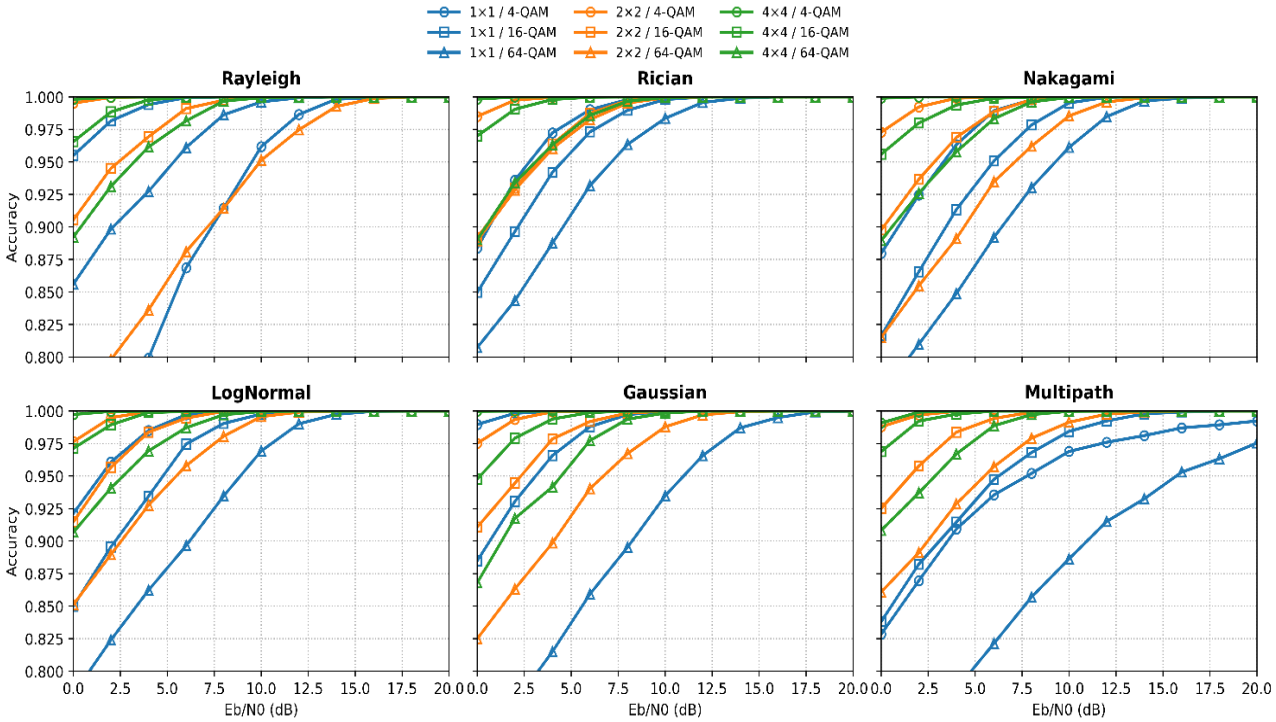

Figure. 3 Accuracies vs Eb/N0 for different channel characteristics vs E_b/N_0 under different numbers of MIMO channel

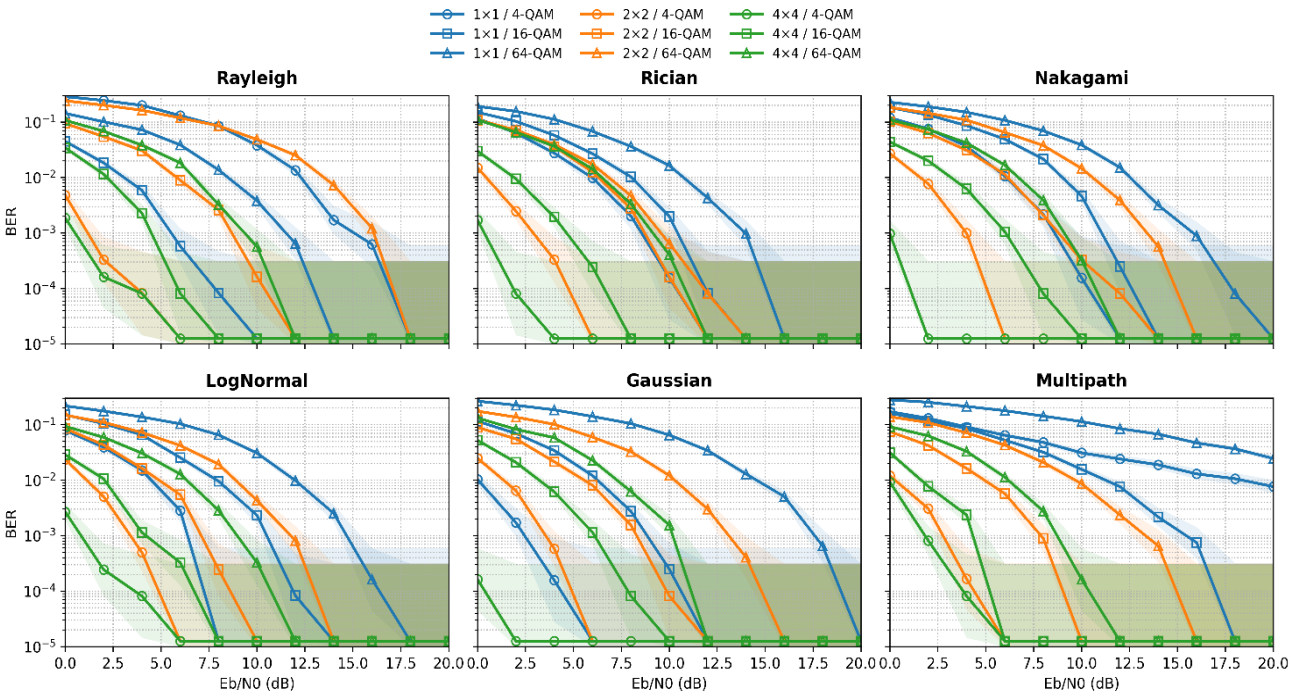

Figure. 4 BER per Eb/N_0 point for different modulation schemes with different MIMO configuration without CSI

Table 8. BER Comparision with related work (2x2 MIMO-OFDM, and 16-QAM, Rayleigh channel, 10 dB)

Method (Year)	Pilots based (J)	10 dB
LS [33]	Yes	1.5×10^{-1}
CNN [28]	yes	8×10^{-1}
CNN-LSTM [31]	Yes	1.9×10^{-4}
Ours: CNN-BRNN	No	8.14×10^{-5}

(FLOPs) with work from literatures. The comparision included different methods in CE starting from traditional methods (e.g., LS and MMSE) moving toward DL based pilot estiation and finally our work with DL with pilotless based CE.

The comparision result highlights that following points, with low number of subcarriers and low MIMO order (i.e., N=64), LS and MMSE FLOP counts considered the lowest. Since both doesn't require large training datasets. But as the number of sub carriers exceed 16K, the proposed CNN-BRNN model reduced the FLOP count by 17% compared to LS and by 94.5% over CNN-LSTM[31]. Increasing the number of FFT subcarriers to 16K is expected when moving toward 5G/6G Massive MIMO to capture frequency selective component. Compared to CNTK[32], our model uses 14.2 times more FLOPs but with using dense number of pilots (J=24). So, the reduction in complexity here is translated into reduction in spectral efficiency and net throughput compared to pilotless method as the proposed in this paper. As N increases the complexity for LS ($O(N^2)$) and MMSE ($O(N^3)$) increases and become more and more expensive. Even for CNTK[32], The complexity is related to the quadratically with pilot number used.

While our proposed model offers complexity of O(N) and becomes more efficient as N increases (e.g., N=16k) without pilot overhead. For better understanding of FLOP count in real-time implementation environment, Table 10 provide examples of different hardware platforms with different processing speed. According to Table 10, each sample can be processed in 4.5ms using Laptop with CPU processor. Moving to GPU further speed up the processing to 0.045ms making real-time CE possible in wideband systems such as 5G/6G.

Fig. 5 compares all six channels with different modulations in 2x2 MIMO configuration with ZF vs. MMSE and Slope-CPE vs Common-CPE. The figure shows the same pattern holds for the two channels: higher-order QAM needs more SNR; MMSE beats ZF by about 0.5–1.5 dB (the biggest difference is in deep fades (i.e., Multipath), where ZF amplifies noise); and slope-CPE is always better than a single common-phase correction, modest in flat channels, about 0.5–1 dB in Multipath. While none of the curves show error floors down to 10^{-5}, which means that the equalization + CPE chain is reliable. The two CPE variants get closer together because of conjugate combining. Comparing these

Table 9. Complexity Comparision with related works by mean of FLOP counts

Method	Complexity order	No of Pilot (J)	FLOPs count		
			$N_t \times N_r$	N=64	N=16K
LS [33]	$O(N^2)$	10	2x2	3.3×10^4	2.14×10^9
			4x4	1.3×10^5	8.58×10^9
MMSE [33]	$O(N^3)$	10	2x2	2.8×10^6	46.9×10^{12}
			4x4	1.1×10^7	18.76×10^{13}
CNN-LSTM [31]	$O(N \times T)$	10	2x2	1.4×10^7	3.26×10^9
			4x4	5.8×10^7	1.3×10^{10}
CNN [28]	$O(J^2 \times M^2 \times T^2)$	10	2x2	1.37×10^7	3.51×10^9
			4x4	5.49×10^7	1.40×10^{10}
CNTK[32]	$O(J^3 + M \times N \times J)$	24	2x2	5.47×10^5	1.259×10^8
			4x4	2.19×10^6	5.03×10^8
Ours: CNN-BRNN	$O(N)$	0	2x2	6.9×10^6	1.78×10^8
			4x4	2.8×10^7	7.14×10^8

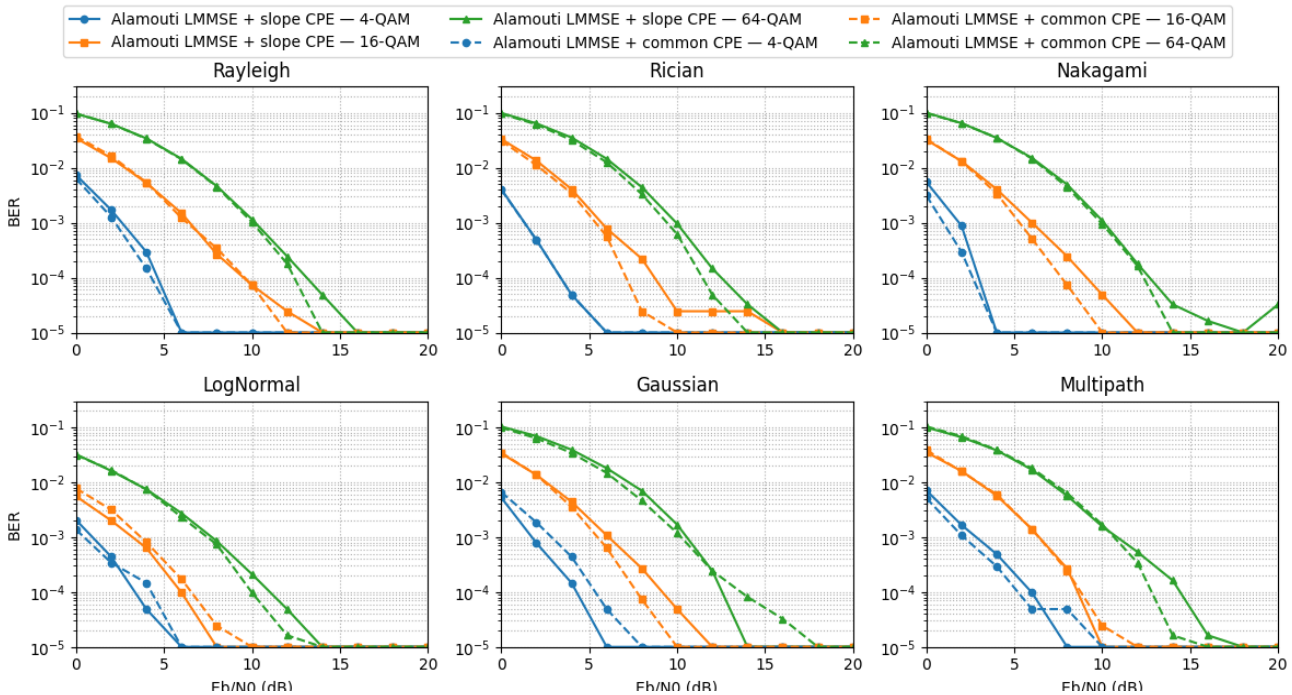

Figure. 5 BER comparison of ZF vs. MMSE and Slope-CPE vs Common-CPE for Alamouti (2x2) with pilot based CSI

curves to the results obtained in Fig.4, without using CSI, we can see that our model is within 1-2 dB behind the hardest cases with 16-QAM for Multipath fading channel. Which represents an achievement considering avoiding the reconstructing of pilot-based H.

7. Conclusions and future suggestions

This paper proposes a low-complexity, data-driven alternative to conventional channel and SNR estimates by employing a LUT discrete supervision to categorize different channels, instead of continuous value CSI target and simultaneously classifying the SNR range. Both estimates come from the received signal and use a CNN-BRNN architecture made up of Conv1D blocks with BN/ReLU and two BRNN layers. CM further provide almost error-free generalization on the evaluated test splits. From a receiver-design point of view, accurate channel/SNR labels make it easier to equalize and detect signals.

The complexity analyses confirm that the proposed CNN-BRNN model achieved lower BER with linear computation complexity growth compared to traditional LS, MMSE and DL based CE, while maintaining real-time deployment capability. The proposed model achieved lower complexity with 45% FLOPs, offering effective and scalable for CE in 5G/6G massive MIMO.

Table 10. Processing time in different hardware (N=16k)

Hardware	Peak FP32	Processing Time/sample
Laptop CPU	100 GFLOP/s	4.5ms
Mid GPU	10 TFLOP/s	0.045ms
Mobile DSP	1 GFLOP/s	447ms

The results also ensure alignment with an authentic OFDM receiver. This methodology enables the application of techniques such as code-aware identification and noise-aware equalization instead of MMSE/LS tap regression.

This results in attributes of accuracy and BER that align with communication theory, particularly regarding the efficacy of QPSK under low SNR and the benefits of 4×4 diversity enhancements. The findings, along with the simple configuration (64-tone OFDM with a 25% CP across six channel types), suggest that this method serves as a beneficial foundation for the development of 5G-class receivers, especially in situations where obtaining pilots is difficult or expensive. This study was performed in a simulated environment utilizing idealized transceivers and six channel models; it did not completely account for hardware imperfections (CFO/phase noise exceeding modelled CPE, IQ imbalance, PA nonlinearity, quantization), rapid Doppler effects, and real-world channel mixtures. SNR was divided into fixed bins, and not all combinations of system parameters (FFT size, CP, pilots, coding, bandwidth, carrier, antenna geometry) were tried out.

In the future, we will test real hardware (SDR/5G testbed) over the air on different channels and while moving to see how well it handles RF problems (CFO/phase noise, IQ/PA nonlinearity) and adjust the model for real-time embedded deployment.

Conflicts of interest

The authors declare that there are no conflicts of interest regarding the publication of this paper.

Author contributions

For this study, the article author contributions are as follows: Yasmine M. Tabra methodology, software, validation, data curation, writing-review and editing. Furat N. Tawfeeq; formal analysis, investigation, resources, writing-original draft preparation.

Appendix A: List of Symbols

Symbol	Description
a_t, b_t	CPE coefficients: phase offset and slope
d_{min}	Minimum Euclidean distance
$e^{\{j(a_t + b_t k)\}}$	CPE phase rotation factor across subcarriers
$H_{(r,n)(k)}$	Channel frequency response
N_c	Length of cyclic prefix (CP)
N_{cp}	Cyclic prefix (CP) length (e.g., 16)
N_0	Noise power spectral density
s_i	Transmitted symbol at antenna/time slot i
$\tilde{s}_t$	Equalized symbol vector estimate
$\hat{s}_{1,k}, \hat{s}_{2,k}$	Estimated Alamouti pair
$\hat{s}_k$	Estimated transmitted symbol
$\hat{x}_{p(n)}$	Time-domain OFDM symbol after IFFT
$x_{cp(n)}$	CP-appended OFDM time samples
$x_{i(k)}$	Transmit symbol from TX antenna
$x_{p(n)}$	Modulated symbol sequence before IFFT
$y_{(r,t)(k)}$	Received vector at RX antenna r
$\omega_{(r,t)(k)}$	Additive white Gaussian noise (AWGN)

References

[1] M.-H. H. and C.-H. We, "Channel estimation for OFDM systems based on comb-type pilot arrangement in frequency selective fading channels", *IEEE Transactions on Consumer Electronics*, Vol. 14, No. 7, pp. 427–440, 1970.

[2] S. Chaurasia and A. Kumar, "OFDM (orthogonal frequency division multiplexing) simulation applying MATLAB", *SSRN Electronic Journal*, No. AECE, pp. 381–386, 2022, doi: 10.2139/ssrn.4157554.

[3] C. Muoghalu, P. Achebe, and A. Ferdinard, "MIMO-OFDM techniques for wireless communication system: Performance evaluation review", *International Journal of Advanced Networking and Applications*, Vol. 14, pp. 5572–5581, 2023, doi: 10.35444/IJANA.2023.14410.

[4] O. Srinivasulu and P. R. Kumar, "Analysis of multiple input multiple output-orthogonal frequency division multiplexing with dynamic optimal power allocation", *Engineering, Technology & Applied Science Research*, Vol. 14, No. 4, pp. 15515–15521, 2024, doi: 10.48084/etasr.7459.

[5] D. Mogylevych and L. Pogrebniak, "Analytical model OFDM-MIMO signal in a radio channel with frequency-time selective fading", *Collection of Information Technology and Security*, Vol. 11, No. 1, pp. 39–46, 2023, doi: 10.20535/2411-1031.2023.11.1.283538.

[6] P. Ramineni, M. Yellagalla, and B. Rajpet, "Evaluation of modulation techniques for 5G

wireless communication: A performance comparison of OFDM, F-OFDM, UFMC and FBMC in terms of PSD, BER and SNR metrics", *Journal of Engineering Research and Reports*, Vol. 26, No. 7, pp. 285–299, 2024, doi: 10.9734/jerr/2024/v26i71209.

[7] Y. O. Imam-Fulani et al., "5G frequency standardization, technologies, channel models, and network deployment: Advances, challenges, and future directions", *Sustainability*, Vol. 15, No. 6, 2023, doi: 10.3390/su15065173.

[8] A. Sharma, "PAPR reduction in the 5G MIMO-OFDM wireless communication system", *International Journal of Engineering Science and Innovative Technology*, Vol. 12, No. 5, pp. 16–20, 2023.

[9] R. K. Mohammed and N. N. Khamiss, "Hybrid multiple access techniques performance analysis of dynamic resource allocation", *Iraqi Journal of Information and Communication Technology*, Vol. 7, No. 1, pp. 23–34, 2024, doi: 10.31987/ijict.7.1.243.

[10] S. Naik Dessai and H. Patidar, "Design and implementation of programmable MIMO FFT OFDM and MIMO DWT OFDM/MIMO FBMC on an embedded platform architecture for 5G applications", *Revista Română de Informatică și Automatică*, Vol. 33, No. 4, pp. 7–20, 2023, doi: 10.33436/v33i4y202301.

[11] D. Abbasi, A. Aziz, and Z. Akram, "Advancements in MIMO antennas for enhanced performance in 5G smartphones communication", *Asian Bulletin of Big Data Management*, Vol. 4, No. 02, pp. 165–177, 2024, doi: 10.62019/abbdm.v4i02.153.

[12] X. Li, Z. Han, H. Yu, L. Yan, and S. Han, "Deep learning for OFDM channel estimation in impulsive noise environments", *Wireless Personal Communications*, Vol. 125, No. 3, pp. 2947–2964, 2022, doi: 10.1007/s11277-022-09693-z.

[13] C. R. Rathish et al., "Enhanced channel prediction in large-scale 5G MIMO-OFDM systems using pyramidal dilation attention convolutional neural network", *Internet Technology Letters*, Vol. 8, No. 1, pp. 1–6, 2024, doi: 10.1002/itl2.532.

[14] C. J. Obagha, C. A. Nwabueze, and C. N. Muoghalu, "Enhancing channel estimation performance for MIMO-OFDM in 5G network using linear minimum mean square error", *International Journal of Engineering and Information Systems*, Vol. 8, No. 8, pp. 100–111, 2024.

[15] D. Adolfsson, "Channel estimation optimization in 5G New Radio using convolutional neural networks", M.Sc. thesis, *Karlstad University*, 2023.

[16] B. Ren, K. Teh, H. An, and E. Gunawan, "MIMO-OFDM modulation classification using 4D2DConvNet for 5G communications", *IEEE Wireless Communications Letters*, Vol. PP, p. 1, 2024, doi: 10.1109/LWC.2024.3394708.

[17] M. Meenalakshmi, S. Chaturvedi, and V. K. Dwivedi, "Deep learning-based channel estimation in 5G MIMO-OFDM systems", in *Proceedings of the 8th International Conference on Signal Processing and Communication (ICSC)*, 2022, pp. 79–84, doi: 10.1109/ICSC56524.2022.10009461.

[18] A. Ranjan and B. C. Sahana, "Deep learning empowered channel estimation in massive MIMO: Unveiling the efficiency of hybrid deep learning architecture", *Journal of Ambient Intelligence and Humanized Computing*, Vol. 16, No. 2, pp. 375–390, 2025, doi: 10.1007/s12652-025-04952-w.

[19] R. Jain, K. Sarvakar, and S. Mishra, "An exhaustive examination of deep learning algorithms: Present patterns and prospects for the future", *Grenze International Journal of Engineering and Technology*, Vol. 10, pp. 105–111, Jan. 2024.

[20] S. Jin, G. Liu, and Q. Bai, "Deep learning in COVID-19 diagnosis, prognosis and treatment selection", *Mathematics*, Vol. 11, No. 6, pp. 1–17, 2023, doi: 10.3390/math11061279.

[21] T. Perumal, N. Mustapha, R. Mohamed, and F. M. Shiri, "A comprehensive overview and comparative analysis on deep learning models", *Journal of Artificial Intelligence*, Vol. 6, No. 1, pp. 301–360, 2024, doi: 10.32604/jai.2024.054314.

[22] I. Cacciari and A. Ranfagni, "Hands-on fundamentals of 1D convolutional neural networks—A tutorial for beginner users", *Applied Sciences*, Vol. 14, No. 18, pp. 1–26, 2024, doi: 10.3390/app14188500.

[23] M. Abd Al Abbas and B. M. Khammas, "Efficient IoT malware detection technique using recurrent neural network", *Iraqi Journal of Information and Communication Technology*, Vol. 7, No. 3, pp. 29–42, 2024, doi: 10.31987/ijict.7.3.249.

[24] D. Qiu, "Research on recurrent neural network recommendation algorithm based on time series", *Applied Computing and Engineering*,

Vol. 87, No. 1, pp. 72–79, 2024, doi: 10.54254/2755-2721/87/20241574.

[25] A. K. Nair and V. Menon, "Joint channel estimation and symbol detection in MIMO-OFDM systems: A deep learning approach using Bi-LSTM", in *Proceedings of the 14th International Conference on Communication Systems and Networks (COMSNETS)*, 2022, pp. 406–411, doi: 10.1109/COMSNETS53615.2022.9668456.

[26] M. Wang, A. Wang, Z. Liu, and J. Chai, "Deep learning based channel estimation method for mine OFDM system", *Scientific Reports*, Vol. 13, No. 1, 2023, doi: 10.1038/s41598-023-43971-5.

[27] Z. Hammed and S. Ameen, "Deep learning based channel estimation for 5G and beyond", *Journal of University of Duhok*, Vol. 26, No. 2, pp. 502–514, 2023, doi: 10.1109/ICICSP59554.2023.10388504.

[28] M. Qasaymeh, A. Alqatawneh, M. A. Khodeir, and A. Aljaafreh, "A deep learning-based approach for channel estimation in multi-access multi-antenna systems", *Journal of Telecommunications and Information Technology*, Vol. 3, pp. 57–64, Sep. 2024, doi: 10.26636/jtit.2024.3.1701.

[29] Y. Singh, P. Swami, V. Bhatia, and P. Brida, "Channel estimation in 5G and beyond networks using deep learning", in *Proceedings of the 34th International Conference Radioelektronika*, 2024, pp. 1–5, doi: 10.1109/RADIOELEKTRONIKA61599.2024.10524095.

[30] Deepanjali S., B. A. J., C. T. Y., and K. A. Reddy, "5G channel estimation using deep learning", *International Journal of Multidisciplinary Research*, Vol. 6, No. 3, pp. 1–9, 2024, doi: 10.36948/ijfmr.2024.v06i03.11040.

[31] S. Vasa, V. Chandrasekhar, and P. N. Kumar, "Deep learning techniques for channel estimation in MIMO-OFDM system for 5G", *Nanotechnology Perceptions*, Vol. 20, No. S8, pp. 704–719, 2024, doi: 10.62441/nano-ntp.v20is8.59.

[32] G. Villemaud and M. Mallik, "Fast channel estimation by infinite width convolutional networks", *Electronics Letters*, Vol. 61, No. 1, pp. 2–7, 2025, doi: 10.1049/ell2.70385.

[33] A. E. Rakhmania, Hudiono, U. A. Ro'isatin, and N. Hidayati, "Channel estimation methods in massive MIMO: A comparative review of machine learning and traditional techniques", *Infocommunications Journal*, Vol. 17, No. 1, pp. 19–31, 2025, doi: 10.36244/ICJ.2025.1.3.

[34] P. Anand and M. K. Arti, "Alamouti-NOMA assisted wireless communication system", *IEEE Access*, Vol. 12, pp. 46104–46108, 2024, doi: 10.1109/ACCESS.2024.3379407.

[35] H. Jafarkhani, "A quasi-orthogonal space-time block code", *IEEE Transactions on Communications*, Vol. 49, No. 1, pp. 1–4, 2001, doi: 10.1109/26.898239.

[36] D. Tse and P. Viswanath, "The wireless channel", in *Fundamentals of Wireless Communication*. Cambridge Univ. Press, 2012, pp. 10–48, doi: 10.1017/CBO9780511807213.003.

[37] J. Yang et al., "Channel fading effect analysis on diffusion cooperation strategies over adaptive networks", *KSII Transactions on Internet and Information Systems*, Vol. 13, No. 1, pp. 172–185, 2019, doi: 10.3837/tiis.2019.01.010.

[38] E. Gómez-Déniz and L. Gómez-Déniz, "A new derivation of the Nakagami-m distribution as a composite of the Rayleigh distribution", *Wireless Networks*, Vol. 30, No. 5, pp. 3051–3060, 2024, doi: 10.1007/s11276-024-03713-5.

[39] J. M. Vallet García, "Characterization of the log-normal model for received signal strength measurements in real wireless sensor networks", *Journal of Sensor and Actuator Networks*, Vol. 9, No. 1, pp. 1–24, 2020, doi: 10.3390/jsan9010012.

[40] S. Kobus, L. Theis, and D. Gündüz, "Gaussian channel simulation with rotated dithered quantization", in *Proceedings of the IEEE International Symposium on Information Theory (ISIT)*, 2024, pp. 1907–1912, doi: 10.1109/ISIT57864.2024.10619428.

[41] G. Gradoni, T. Chen, M. You, A. Walker, Y. Zheng, and F. Burton, "Interference mitigation in wireless communications assisted by reconfigurable intelligent surfaces", in *Proceedings of the 2024 IEEE INC-USNC-URSI Radio Science Meeting (Joint with AP-S Symposium)*, 2024, p. 369, doi: 10.23919/INC-USNC-URSI61303.2024.10632500.